Experimental Demonstration of High-Rate Measurement-Device-Independent Quantum Key Distribution over Asymmetric Channels

Hui Liu,[1,2,*] Wenyuan Wang,[3,*] Kejin Wei,[1,2] Xiao-Tian Fang,[1,2] Li Li,[1,2] Nai-Le Liu,[1,2] Hao Liang,[1,2] Si-Jie Zhang,[1,2] Weijun Zhang,[4] Hao Li,[4] Lixing You,[4] Zhen Wang,[4] Hoi-Kwong Lo,[3] Teng-Yun Chen,[1,2] Feihu Xu,[1,2] and Jian-Wei Pan[1,2]

[1]*Shanghai Branch, Hefei National Laboratory for Physical Sciences at Microscale and Department of Modern Physics, University of Science and Technology of China, Shanghai 201315, China*

[2]*CAS Center for Excellence and Synergetic Innovation Center in Quantum Information and Quantum Physics, University of Science and Technology of China, Shanghai 201315, People's Republic of China*

[3]*Centre for Quantum Information and Quantum Control (CQIQC), Department of Electrical & Computer Engineering and Department of Physics, University of Toronto, Toronto, Ontario M5S 3G4, Canada*

[4]*State Key Laboratory of Functional Materials for Informatics, Shanghai Institute of Microsystem and Information Technology, Chinese Academy of Sciences, Shanghai 200050, China*

(Received 6 September 2018; published 26 April 2019)

Measurement-device-independent quantum key distribution (MDI-QKD) can eliminate all detector side channels and it is practical with current technology. Previous implementations of MDI-QKD all used two symmetric channels with similar losses. However, the secret key rate is severely limited when different channels have different losses. Here we report the results of the first high-rate MDI-QKD experiment over *asymmetric* channels. By using the recent 7-intensity optimization approach, we demonstrate $> 10\times$ higher key rate than the previous best-known protocols for MDI-QKD in the situation of large channel asymmetry, and extend the secure transmission distance by more than 20–50 km in standard telecom fiber. The results have moved MDI-QKD towards widespread applications in practical network settings, where the channel losses are asymmetric and user nodes could be dynamically added or deleted.

DOI: 10.1103/PhysRevLett.122.160501

Quantum key distribution (QKD) promises information-theoretical security in communications [1,2]. In practice, however, the realistic QKD implementations might introduce device imperfections [3], which deviate from the idealized models [4–9]. Among many protocols to resolve the device imperfections [10–12], the measurement-device-independent QKD (MDI-QKD) protocol [13] has attracted a lot of research interest due to its practicality with current technology and its natural advantage of immunity to all detector attacks. Experimental MDI-QKD [14–20] has advanced significantly up to a distance of 404 km in low loss fiber [21] and a key rate of 1 Mbit/s [22]. Many theoretical improvements have been proposed to guarantee the practical security [23–28]. Notably, the recent proposal of twin-field QKD has the capability to overcome the rate-distance limit of QKD [29].

The future of QKD is believed to be a quantum network in which many user nodes are connected together via quantum channels and centric servers, such as the star-type network illustrated in Fig. 1. MDI-QKD is well suited to construct such a centric QKD network even with an untrusted relay; i.e., the six users in Fig. 1 can securely communicate with each other, though Charlie is insecure. Such a MDI-QKD network, as demonstrated in Ref. [30], presents a huge advantage over traditional trusted-relay based QKD networks [31–33].

In a practical quantum network, it is inevitable that some users are further away from the central relay, while others are closer to the relay. For instance, in Fig. 1, user 1 and user 3 are farther from Charlie than the other users. This topology has appeared naturally in previous field QKD networks [31–33]. Unfortunately, so far, all implementations to MDI-QKD have

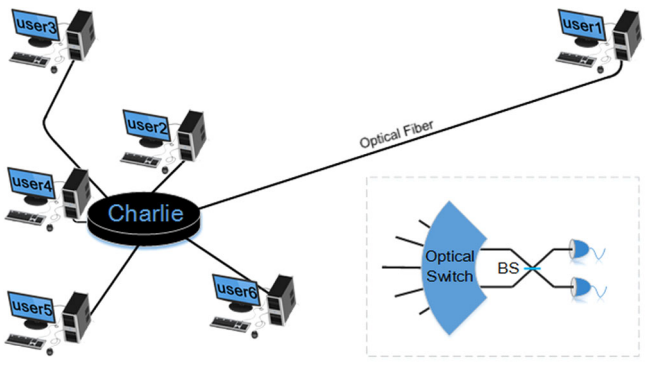

FIG. 1. An illustration of a star-type MDI-QKD network providing six users with access to the untrusted relay, Charlie. Inset: an example of the possible implementation by Charlie.

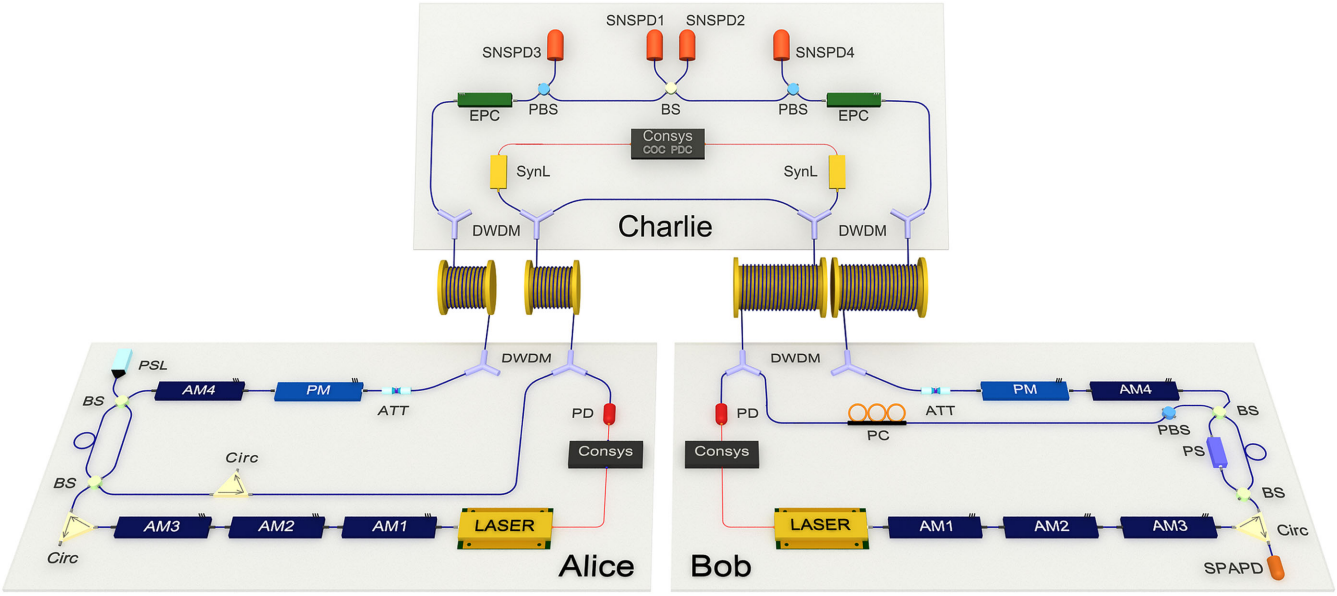

FIG. 2. MDI-QKD setup. Alice's (Bob's) signal laser pulses are modulated into signal and decoy intensities by three amplitude modulators (AM1-AM3). Key bits are encoded by a Mach-Zehnder interferometer, AM4, and a phase modulator (PM). In Charlie, the polarization stabilization system in each link includes an electric polarization controller (EPC), a polarization beam splitter (PBS) and a superconducting nanowire single-photon detector (SNSPD); the Bell state measurement (BSM) system includes a 50/50 beam splitter (BS), SNSPD1 and SNSPD2. Abbreviations of other components: DWDM, dense wavelength division multiplexer; ConSys, control system; ATT, attenuator; PSL, phase-stabilization laser; Circ, circulator; PC, polarization controller; PS, phase shifter; SPAPD, single-photon avalanche photodiode.

been performed either through near-symmetric channels [15–20] or through the deliberate addition of loss in one channel to balance the total losses in the two arms [14]. However, the assumption of near-symmetric channels is clearly an unsatisfactory situation in a practical MDI-QKD network. Adding loss in one channel will severely limit the key rate and the secure distance in the asymmetric setting [25], and it also means that the addition or deletion of a new node will inevitably affect every other existing node, which is highly inconvenient and limits the scalability of the network.

We, for the first time, demonstrate high-rate MDI-QKD over asymmetric channels and achieve substantially higher key rate over previous methods for MDI-QKD. Our experiment employs the 7-intensity optimization method proposed recently in Ref. [34]. We demonstrate that the 7-intensity method can be implemented in software only without having to physically modify any channel, and it is highly scalable and can be easily integrated into existing quantum network infrastructure.

TABLE I. List of parameters characterized from experiment: detector dark count rate Y_0, detector system efficiency η_d, optical misalignment e_d^X, e_d^Z in the X and Z bases, fiber loss coefficient α in dB/km, error-correction efficiency f, security parameter ϵ, and the total number of laser pulses N sent by Alice or Bob.

Y_0	η_d	e_d^Z	e_d^X	α	f	ϵ	N
6.40×10^{-8}	46%	0.5%	4%	0.19	1.16	10^{-10}	10^{12}

In asymmetric MDI-QKD with two users, Alice and Bob have channel transmittances η_A and η_B ($\eta_A \neq \eta_B$). The main question is how to choose the optimal intensities of the weak coherent pulses for Alice and Bob, denoted by s_A and s_B, so as to maximize the key rate [25]. A natural option is to choose the intensities to balance the channel losses, i.e., $s_A\eta_A = s_B\eta_B$. By doing so, a symmetry of photon flux can arrive at Charlie, and thus result in a good Hong-Ou-Mandel (HOM) dip [35]. The dependency of HOM visibility vs balance of photon number flux can be seen in Refs. [34,36]. However, such an option is suboptimal, and may even generate no key rate at all when the channel asymmetry is high. The fundamental reason is that MDI-QKD is related but *different* from HOM dip. That is, HOM dip affects only the errors in the X basis (i.e., the phase error rate estimated with the decoy state method), but has no effect to errors in the Z basis (i.e., the bit error rate). Therefore, the optimal method is to decouple the decoy state estimation in the X basis from key generation in the Z basis. This is the key idea of the 7-intensity optimization method proposed in Ref. [34]. Note that Ref. [28] also mentioned on passing the possibility of using different intensities for Alice and Bob, but no analysis on this important asymmetric case was performed there.

In the 7-intensity optimization method [34], Alice and Bob each select a set of 4 intensities, namely, a signal state $\{s_A, s_B\}$ in the Z basis, and decoy states $\{\mu_A, \nu_A, \omega\}$ and $\{\mu_B, \nu_B, \omega\}$ in the X basis, respectively. The parameters that Alice and Bob choose include 7 different intensities in total,

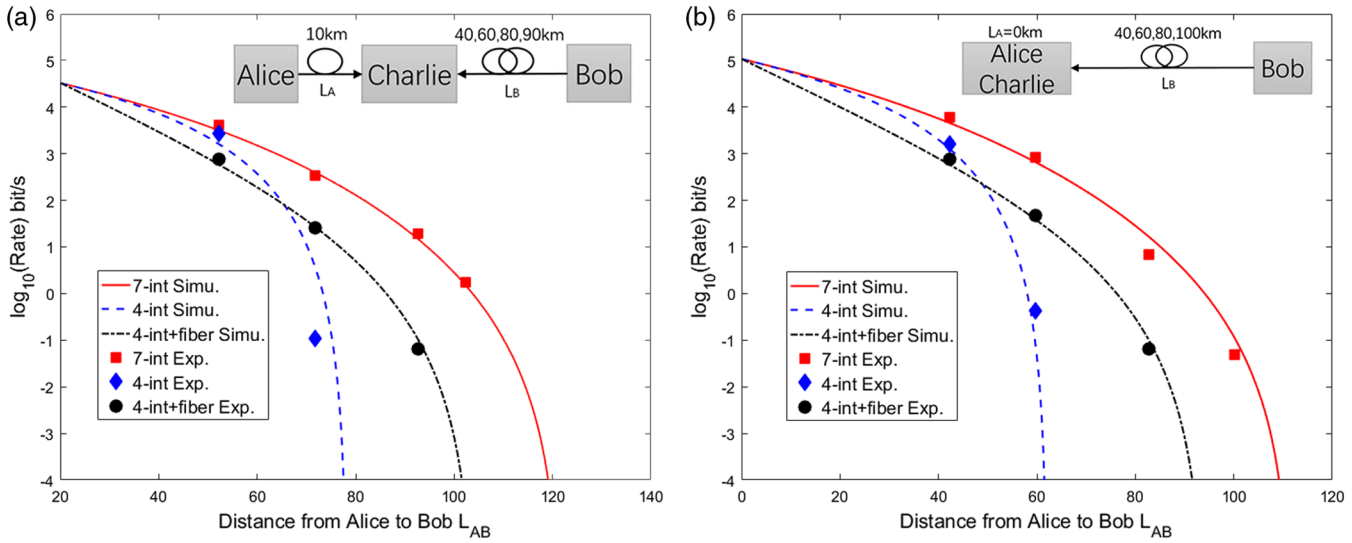

FIG. 3. Simulation (curve) and experiment results (data points) for secret rate (bit/pulse) vs the total distance L_{AB} in standard telecom fiber. (a) L_A is fixed at 10 km, while L_B is selected at 40, 60, 80, and 90 km. (b) L_A is fixed at 0 km, while L_B is selected at 40, 60, 80, and 100 km. The points (curves) in the figure indicate the experimental (simulation) results for (i) the 4-intensity method shown as blue diamonds (blue dashed line), where the same intensities and proportions for Alice and Bob are selected and optimized in the 4-intensity protocol [21,28]; (ii) the 4-intensity + fiber method [14] shown as black dots (black dot-dash line); (iii) the 7-intensity method [34], shown in red squares (red solid line). As can be seen, for the 4-intensity methods, adding fibers improves the key rate in long distances, but it does not in short distances. In contrast, the 7-intensity method always achieves a substantially higher key rate than any of the other two methods, especially when channel asymmetry is high.

as well as the proportions to send them. The secret key is generated only from the Z basis, while the data in the X basis are all used to perform the decoy state analysis. The decoy state intensities are chosen to compensate for asymmetry and ensure good HOM visibility in the X basis (and roughly satisfy $(\mu_A/\mu_B) = (\nu_A/\nu_B) \approx (\eta_B/\eta_A)$, which maintains symmetry of the photon flux arriving at Charlie). On the other hand, the signal state is decoupled from the decoy states, and can be freely adjusted to maximize the key rate in the Z basis (and, generally, $(s_A/s_B) \neq (\eta_B/\eta_A)$). Overall, Alice and Bob optimize 12 implementation parameters: $[s_A, \mu_A, \nu_A, p_{s_A}, p_{\mu_A}, p_{\mu_A}, s_B, \mu_B, \nu_B, p_{s_B}, p_{\mu_B}, p_{\mu_B}]$. To efficiently choose the optimal parameters, we use a local search algorithm and follow the optimization technique in Ref. [34], which converts the 12 parameters into polar coordinates and searches them while locking the decoy state intensities at $(\mu_A/\nu_A) = (\mu_B/\nu_B)$ [37]. The optimization technique is highly efficient, and takes less than 0.1 s for each run of full optimization on a common desktop PC (with a quad-core Intel i7-4790k processor, using parallelization with 8 threads).

To implement MDI-QKD over two asymmetric channels, we construct a time-bin-phase encoding MDI-QKD setup in Fig. 2. Alice and Bob each possess an internally modulated laser which emits phase-randomized laser pulses at a clock rate of 75 MHz. The gain-switched laser diode can naturally generate optical pulses with random phases. AM1 (amplitude modulator) is used to tailor the pulse shape by cutting off the overshoot rising edge of laser pulses. AM2 and AM3 are employed to randomly modulate the intensities of the signal state and weak decoy states. The time-bin encoding is implemented by utilizing a combination of a Mach-Zehnder interferometer (MZI), AM4, and a phase modulator (PM). For the Z basis, the key bit is encoded in time bin $|0\rangle$ or $|1\rangle$ by AM4, while for the X basis, it is encoded in the relative phase 0 or π by the PM. Alice and Bob send their laser pulses through two standard fiber spools, L_A and L_B, to Charlie, who performs Bell state measurement (BSM). The BSM includes a 50/50 beam splitter (BS) and two superconducting nanowire single-photon detectors (SNSPD1 and SNSPD2). The main system parameters characterized in the experiment are shown in Table I.

To compensate for the relative phase drift and establish a common phase reference, Alice employs a phase-stabilization laser (PSL) and Bob employs a phase shifter (PS) in one of the arms of his MZI and a single-photon avalanche photodiode. To properly interfere the two pulses at Charlie, we develop a real-time polarization feedback control system, an automatic time calibration system and a temperature feedback control system [37]. Thanks to the feedback control systems, the observed visibility of the two photon interference is about 46% and the system has a long-term stability over tens of hours. This stability enables us to collect a large number of signal detections, thus properly considering the finite-key effect [26].

We implement the 7-intensity method over different choices of channel lengths [37]. First, we fix the distance

between Alice and Charlie at 10 km, i.e., $L_A = 10$ km, while the distance between Bob and Charlie, L_B, varies from 40 to 90 km. At each channel setting, we use the system parameters listed in Table I to perform a numerical optimization on the implementation parameters, based on three optimization strategies: (i) the 4-intensity method, where the same intensities and proportions for Alice and Bob are selected and optimized in the 4-intensity protocol [21,28]; (ii) the 4-intensity + fiber method, where the asymmetry of channels is first compensated by adding additional losses [14] and then the same intensities and proportions for Alice and Bob are selected; (iii) the 7-intensity method. The results are shown in Fig. 3(a). The 7-intensity method can substantially increase the key rate and maximum distance of MDI-QKD in the case of high channel asymmetry: at $L_B = 60$ km, the 7-intensity method generates a secret key rate of over an order of magnitude higher than the 4-intensity + fiber method, and extends the maximum distance for approximately 20 km compared to the 4-intensity + fiber method, and 40 km compared to the 4-intensity method alone.

Next, we demonstrate for the first time a "single-arm" MDI-QKD, as shown in the inset figure in Fig. 3(b), where we place Alice and Charlie at the same location, i.e., $L_A = 0$ km. L_B varies from 40 to 100 km. The results are shown in Fig. 3(b). Such a single-arm setup only uses one public channel, and could be highly useful in free-space QKD, where Alice and Bob typically have a single free-space channel, in the middle of which adding a relay is unfeasible (e.g., ship-to-ship or satellite-ground channel). In this case, adding fiber in the lab would also be inconvenient due to turbulence or moving platforms. Using single-arm MDI-QKD, however, Bob can place a relay in his lab, such that Alice and Bob can enjoy the security of MDI-QKD through this channel, and maintain a satisfactory key rate.

We list the implementation parameters and the main experimental results for $L_A = 10$ and $L_B = 60$ km in Table II. Note that the parameters in the 7-intensity method are quite different from those two types of 4-intensity methods. We obtain a secret key rate of 343 bits/s with the 7-intensity method, which is 13.5 times higher than that of the 4-intensity + fiber method. By using the joint-bound analysis [28], the key rate can be further improved to 645 bits/s. Moreover, the 7-intensity optimization method can greatly extend the transmission distance by about 50 km fiber. Furthermore, we also tested an extreme case where $L_A = 0$ and $L_B = 100$ km. 7-intensity produces a secret key rate of 0.049 bit/s. In contrast, no key bits can be extracted with either strategy of using the 4-intensity method with/without fiber.

The method of asymmetric intensities and decoupled bases we demonstrated can be applied to general quantum information protocols. First, the asymmetric method is important to the future implementation of free-space MDI-QKD with a moving relay such as satellite. For instance, the channel transmittances in satellite-based quantum communication are constantly changing with up to 20-dB channel mismatch [38]. Second, the asymmetric method can be readily applied to MDI quantum digital signature (QDS) [39–41] and twin-field (TF) QKD [29]. The key generation formula of MDI-QDS is similar to that of MDI-QKD, where the proposed method can be directly implemented [37]. TF-QKD relies on single-photon interference, where the intensity-asymmetry affects both the interference visibility and the single-photon gain [37]. Our methods of asymmetric choice of intensities and optimization of parameters can be implemented to improve the key rate for asymmetric TF-QKD [42]. However, we note that the two encoding bases are symmetric in TF-QKD; thus the method of decoupled bases might not be applicable [37]. Finally, other protocols that rely on single-photon or two-photon interference, such as comparison of coherent states [43] and quantum fingerprinting [44–46], can also benefit from our methods when they are working in an asymmetric setting.

In conclusion, by using the recent 7-intensity method, we demonstrate an order of magnitude higher key rate and an extension of 20–50 km distance over previous best-known MDI-QKD protocols. While previous methods of adding fibers inconveniently require the modification of every existing node with the addition or deletion of a new node, our 7-intensity method implements the optimization in software

TABLE II. Example implementation parameters and experimental results for $L_A = 10$ and $L_B = 60$ km. s_{11}^Z is the estimated yield of single photons in the Z basis and e_{11}^X is the estimated phase-flip error rate of single photons in the X basis. Q_{ss}^Z and E_{ss}^Z are the observed gain and QBER for signal states. R is the secret key rate (bit/s). Ratio is the key rate advantage of the 7-intensity method over the given method.

Parameters	7-intensity	4-intensity	4-intensity + fiber
s_A	0.169	0.119	0.363
s_B	0.614	0.119	0.363
μ_A	0.056	0.180	0.280
μ_B	0.465	0.180	0.280
ν_A	0.011	0.023	0.058
ν_B	0.089	0.023	0.058
p_{s_A}	0.599	0.256	0.483
p_{s_B}	0.600	0.256	0.483
p_{μ_A}	0.030	0.035	0.045
p_{μ_B}	0.031	0.035	0.045
p_{ν_A}	0.254	0.490	0.320
p_{ν_B}	0.248	0.490	0.320
s_{11}^Z	1.63×10^{-3}	1.97×10^{-3}	1.86×10^{-4}
e_{11}^X	14.00%	20.28%	16.72%
Q_{ss}^Z	2.24×10^{-4}	3.05×10^{-5}	3.10×10^{-5}
E_{ss}^Z	0.91%	2.50%	0.91%
R	343	0.11	25.50
Ratio	1	3118	13.5

only and provides much better scalability. Overall, our results have moved MDI-QKD towards a more practical network setting, where the channel losses can be asymmetric and nodes can be dynamically added or deleted.

This work has been supported by the National Key R&D Program of China (2018YFB0504303, 2017YFA0304003, 2017YFA0303903), National Natural Science Foundation of China (Grants No. 61771443, No. 61875182, No. 61705048), Anhui Initiative in Quantum Information Technologies, Fundamental Research Funds for the Central Universities (WK2340000083), Shanghai Science and Technology Development Funds (18JC1414700). F. X. acknowledges the support from Thousand Young Talent program of China. W. W. and H.-K. L. were supported by NSERC, U.S. Office of Naval Research, CFI, ORF, and Huawei Canada.

[*] These author contributed equally to this work.

[1] C. H. Bennett and G. Brassard, in *Proceedings of the IEEE International Conference on Computer, Systems & Signal Processing, Bangalore, India, 1984* (IEEE, New York, 1984), p. 175.
[2] A. K. Ekert, Phys. Rev. Lett. **67**, 661 (1991).
[3] F. Xu, X. Ma, Q. Zhang, H.-K. Lo, and J.-W. Pan, arXiv:1903.09051.
[4] Y. Zhao, C.-H. Fung, B. Qi, C. Chen, and H.-K. Lo, Phys. Rev. A **78**, 042333 (2008).
[5] F. Xu, B. Qi, and H.-K. Lo, New J. Phys. **12**, 113026 (2010).
[6] L. Lydersen, C. Wiechers, C. Wittmann, D. Elser, J. Skaar, and V. Makarov, Nat. Photonics **4**, 686 (2010).
[7] I. Gerhardt, Q. Liu, A. Lamas-Linares, J. Skaar, C. Kurtsiefer, and V. Makarov, Nat. Commun. **2**, 349 (2011).
[8] W. Henning, K. Harald, R. Markus, F. Martin, N. Sebastian, and W. Harald, New J. Phys. **13**, 073024 (2011).
[9] N. Jain, C. Wittmann, L. Lydersen, C. Wiechers, D. Elser, C. Marquardt, V. Makarov, and G. Leuchs, Phys. Rev. Lett. **107**, 110501 (2011).
[10] D. Mayers and A. Yao, in *Proceedings of the 39th Annual Symposium on Foundations of Computer Science* (IEEE Computer Society, Washington, DC, 1998), p. 503.
[11] A. Acín, N. Brunner, N. Gisin, S. Massar, S. Pironio, and V. Scarani, Phys. Rev. Lett. **98**, 230501 (2007).
[12] S. L. Braunstein and S. Pirandola, Phys. Rev. Lett. **108**, 130502 (2012).
[13] H.-K. Lo, M. Curty, and B. Qi, Phys. Rev. Lett. **108**, 130503 (2012).
[14] A. Rubenok, J. A. Slater, P. Chan, I. Lucio-Martinez, and W. Tittel, Phys. Rev. Lett. **111**, 130501 (2013).
[15] T. F. da Silva, D. Vitoreti, G. B. Xavier, G. C. do Amaral, G. P. Temporao, and J. P. von der Weid, Phys. Rev. A **88**, 052303 (2013).
[16] Y. Liu, T. Y. Chen, L. J. Wang, H. Liang, G. L. Shentu, J. Wang, K. Cui, H. L. Yin, N. L. Liu, L. Li, X. F. Ma, J. S. Pelc, M. M. Fejer, C. Z. Peng, Q. Zhang, and J. W. Pan, Phys. Rev. Lett. **111**, 130502 (2013).
[17] Z. Tang, Z. Liao, F. Xu, B. Qi, L. Qian, and H.-K. Lo, Phys. Rev. Lett. **112**, 190503 (2014).
[18] Y.-L. Tang, H.-L. Yin, S.-J. Chen, Y. Liu, W.-J. Zhang, X. Jiang, L. Zhang, J. Wang, L.-X. You, J.-Y. Guan, D.-X. Yang, Z. Wang, H. Liang, Z. Zhang, N. Zhou, X. Ma, T.-Y. Chen, Q. Zhang, and J.-W. Pan, Phys. Rev. Lett. **113**, 190501 (2014).
[19] C. Wang, X.-T. Song, Z.-Q. Yin, S. Wang, W. Chen, C.-M. Zhang, G.-C. Guo, and Z.-F. Han, Phys. Rev. Lett. **115**, 160502 (2015).
[20] Z. Tang, K. Wei, O. Bedroya, L. Qian, and H.-K. Lo, Phys. Rev. A **93**, 042308 (2016).
[21] H.-L. Yin, T.-Y. Chen, Z.-W. Yu, H. Liu, L.-X. You, Y.-H. Zhou, S.-J. Chen, Y. Mao, M.-Q. Huang, W.-J. Zhang, H. Chen, M. J. Li, D. Nolan, F. Zhou, X. Jiang, Z. Wang, Q. Zhang, X.-B. Wang, and J.-W. Pan, Phys. Rev. Lett. **117**, 190501 (2016).
[22] L. C. Comandar, M. Lucamarini, B. Frhlich, J. F. Dynes, A. W. Sharpe, S. W. B. Tam, Z. L. Yuan, R. V. Penty, and A. J. Shields, Nat. Photonics **10**, 312 (2016).
[23] X. Ma, C.-H. F. Fung, and M. Razavi, Phys. Rev. A **86**, 052305 (2012).
[24] X.-B. Wang, Phys. Rev. A **87**, 012320 (2013).
[25] F. Xu, M. Curty, B. Qi, and H.-K. Lo, New J. Phys. **15**, 113007 (2013).
[26] M. Curty, F. Xu, W. Cui, C. C. W. Lim, K. Tamaki, and H.-K. Lo, Nat. Commun. **5**, 3732 (2014).
[27] F. Xu, H. Xu, and H.-K. Lo, Phys. Rev. A **89**, 052333 (2014).
[28] Y.-H. Zhou, Z.-W. Yu, and X.-B. Wang, Phys. Rev. A **93**, 042324 (2016).
[29] M. Lucamarini, Z. Yuan, J. Dynes, and A. Shields, Nature (London) **557**, 400 (2018).
[30] Y.-L. Tang, H.-L. Yin, Q. Zhao, H. Liu, X.-X. Sun, M.-Q. Huang, W.-J. Zhang, S.-J. Chen, L. Zhang, L.-X. You, Z. Wang, Y. Liu, C.-Y. Lu, X. Jiang, X. Ma, Q. Zhang, T.-Y. Chen, and J.-W. Pan, Phys. Rev. X **6**, 011024 (2016).
[31] M. Peev *et al.*, New J. Phys. **11**, 075001 (2009).
[32] T.-Y. Chen, J. Wang, H. Liang, W.-Y. Liu, Y. Liu, X. Jiang, Y. Wang, X. Wan, W.-Q. Cai, and L. Ju, Opt. Express **18**, 27217 (2010).
[33] M. Sasaki, M. Fujiwara, H. Ishizuka, W. Klaus, K. Wakui, M. Takeoka, S. Miki, T. Yamashita, Z. Wang, and A. Tanaka, Opt. Express **19**, 10387 (2011).
[34] W. Wang, F. Xu, and H.-K. Lo, arXiv:1807.03466.
[35] C.-K. Hong, Z.-Y. Ou, and L. Mandel, Phys. Rev. Lett. **59**, 2044 (1987).
[36] E. Moschandreou, J. I. Garcia, B. J. Rollick, B. Qi, R. Pooser, and G. Siopsis, J. Lightwave Technol. **36**, 3752 (2018).
[37] See Supplemental Material at http://link.aps.org/supplemental/10.1103/PhysRevLett.122.160501 for the details of the optimization algorithm, the MDI-QKD setup, the implementation parameters, the experimental results, and the application of the asymmetric approach to other protocols.
[38] J. Yin, Y. Cao, Y.-H. Li, S.-K. Liao, L. Zhang, J.-G. Ren, W.-Q. Cai, W.-Y. Liu, B. Li, and H. Dai *et al.*, Science **356**, 1140 (2017).
[39] I. V. Puthoor, R. Amiri, P. Wallden, M. Curty, and E. Andersson, Phys. Rev. A **94**, 022328 (2016).
[40] G. Roberts, M. Lucamarini, Z. Yuan, J. Dynes, L. Comandar, A. Sharpe, A. Shields, M. Curty, I. Puthoor, and E. Andersson, Nat. Commun. **8**, 1098 (2017).

[41] H.-L. Yin *et al.*, Phys. Rev. A **95**, 042338 (2017).
[42] X. Zhou, C. Zhang, C. Zhang, and Q. Wang, arXiv:1902.03385.
[43] E. Andersson, M. Curty, and I. Jex, Phys. Rev. A **74**, 022304 (2006).
[44] J. M. Arrazola and N. Lütkenhaus, Phys. Rev. A **89**, 062305 (2014).
[45] F. Xu, J. M. Arrazola, K. Wei, W. Wang, P. Palacios-Avila, C. Feng, S. Sajeed, N. Lütkenhaus, and H.-K. Lo, Nat. Commun. **6**, 8735 (2015).
[46] J.-Y. Guan, F. Xu, H.-L. Yin, Y. Li, W.-J. Zhang, S.-J. Chen, X.-Y. Yang, L. Li, L.-X. You, T.-Y. Chen *et al.*, Phys. Rev. Lett. **116**, 240502 (2016).